Biochemistry

pubs.acs.org/biochemistry Article

Tuning Allostery through Integration of Disorder to Order with a Residue Network

Jingheng Wang,[‖] Riya Samanta,[‖] Gregory Custer, Christopher Look, Silvina Matysiak, and Dorothy Beckett*

Cite This: *Biochemistry* 2020, 59, 790–801 Read Online

ACCESS | Metrics & More | Article Recommendations | Supporting Information

ABSTRACT: In allostery, a signal from one site in a protein is transmitted to a second site to alter its function. Due to its ubiquity in biology and the potential for its exploitation in drug and protein design, the molecular basis of allosteric communication continues to be the subject of intense research. Although allosterically coupled sites are frequently characterized by disorder, how communication between disordered segments occurs remains obscure. Allosteric activation of *Escherichia coli* BirA dimerization occurs via coupled distant disorder-to-order transitions. In this work, combined structural and computational studies reveal an extensive residue network in BirA. Substitution of several network residues yields large perturbations to allostery. Force distribution analysis reveals that disruptions to the disorder-to-order transitions through amino acid substitution are manifested in shifts in the energy experienced by network residues as well as alterations in packing of an α-helix that plays a critical role in allostery. The combined results reveal a highly distributed allosteric mechanism that is robust to sequence change.

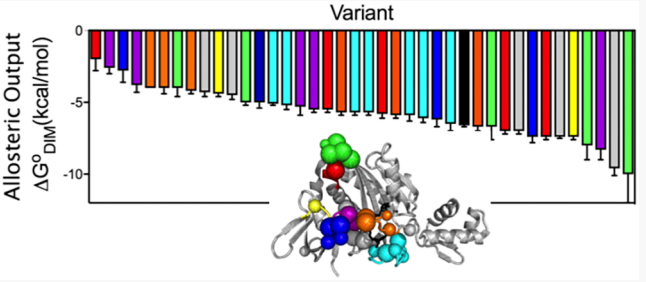

Allostery, or energetic coupling between events that occur at distinct sites in a protein, is a widespread phenomenon. As "the second secret of life",[1] it is utilized in virtually all of biology, including metabolism,[2] cell signaling,[3] and transcription regulation.[4] Consequently, its molecular basis remains the subject of intense research. Although many studies have highlighted the importance of disorder for the thermodynamics of protein allostery,[5−7] the physicochemical basis of long-range energetic coupling between disordered protein segments remains to be elucidated.

The *Escherichia coli* biotin protein ligase (BirA, UniPROT, BIRA_ECOLI, P06709) provides a system for determining how disorder-to-order transitions are communicated in allostery. The protein is a transcription repressor that is allosterically activated for homodimerization via biotinyl 5′-adenylate (bio-5′-AMP) binding.[8] The resulting holoBirA homodimer binds to DNA to repress transcription of the biotin biosynthetic operon.[9,10] Structural studies reveal that bio-5′-AMP binding is accompanied by disorder-to-order transitions on the coupled ligand binding and dimerization surfaces, which are separated by >30 Å (Figure 1[11−13]). The adenylate and biotin binding loops (ABL and BBL, respectively) on the ligand binding surface are disordered in apoBirA but fold around bio-5′-AMP in the holorepressor. On the dimerization surface, effector binding is coupled to extension of an α-helix and ordering/packing of two loop segments. Functional measurements performed on BirA variants with amino acid substitutions indicate critical roles of disorder-to-order transitions on each functional surface for allostery[14−16] and coupling of the distant folding processes.[17,18] The molecular mechanism of this coupling is unknown.

Results of previous studies suggest that a number of electrostatic residues may contribute to BirA allostery.[19] Inspection of the holoBirA structure reveals that the effector nucleates multiple interactions involving charged/polar amino acid side chains (Figure 1B). Only a subset of the observed interactions have a high likelihood of forming in apoBirA because in the absence of ligand the BBL, which contains residues R118, R119, and R121, is disordered.[11,12] Analysis of molecular dynamics (MD) simulation trajectories revealed that an alanine substitution that perturbs folding on the ligand binding surface and bio-5′-AMP-linked dimerization also disrupts interactions involving residue R118.[19] Additionally, analysis of the simulation trajectories obtained for BirA variants with single-amino acid substitutions in the core predicts correlation of rearrangement of the electrostatic interaction network with altered bio-5′-AMP binding-linked dimerization.[19] Although these previous studies implicate an electrostatic residue network in BirA allostery, the full scope of

Received: November 12, 2019
Revised: January 3, 2020
Published: January 3, 2020

https://dx.doi.org/10.1021/acs.biochem.9b01006
Biochemistry 2020, 59, 790−801

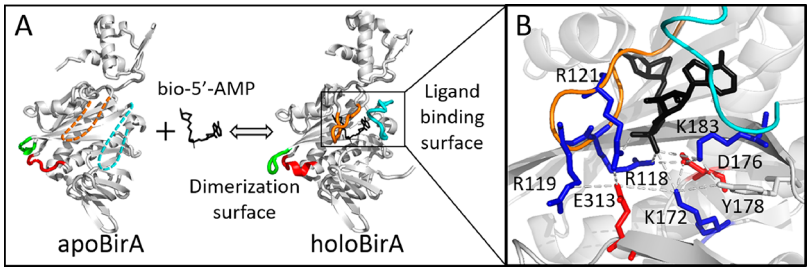

Figure 1. Structural analysis of disorder-to-order and network formation upon bio-5′-AMP binding to BirA. (A) BirA structures with loop disorder-to-order transitions highlighted: residues 140−146 (red), residues 193−199 (green), BBL (orange), and ABL (cyan). The dashed segments indicate disorder. (B) Network interactions in holoBirA with the following side chain color codes: red, negatively charged; blue, positively charged; black, ligand. Models were created in Pymol with Protein Data Bank entries 1BIA and 2EWN as input.

the network, its functional significance, and its role in coupling disorder-to-order transitions on the ligand binding and dimerization surfaces remain to be determined.

In this work, we applied computation and experiment to identify an energy-based residue network in BirA, to determine the function of the network, and to elucidate how the network is integrated with the disorder-to-order transitions in BirA allostery. Computational analysis reveals a residue network more extensive than that extracted from structural analysis. Measurements of proton linkage to effector binding support network formation in solution. Results of ITC and sedimentation equilibrium measurements reveal that disruption of the network by alanine substitution significantly perturbs both allosteric effector binding and effector-linked dimerization. Finally, force distribution analysis reveals that the network is directly linked to disorder-to-order transitions on the two functional surfaces. The results support a highly distributed mechanism in which allosteric communication is accomplished through integration of a residue network with local folding events and general compaction of the protein.

MATERIALS AND METHODS

Chemicals and Biochemicals. All chemicals and biochemicals were at least reagent grade. The d-biotin (Sigma-Aldrich) stock solutions were prepared in standard buffer [10 mM Tris (pH 7.50 ± 0.02 at 20 °C), 200 mM KCl, and 2.5 mM $MgCl_2$] and stored in −80 °C. The biotinoyl 5′-adenylate (bio-5′-AMP) was synthesized and purified as previously described,[9,20] and the bio-5′-AMP analogue, biotinol 5′-adenylate (btnOH-AMP), was purchased from RNA-Tech (Leuven, Belgium). The btnOH-AMP and bio-5′-AMP stock solutions, which were stored at −80 °C, were prepared by dissolving the dry powder into Milli-Q water. Concentrations were determined by absorption spectroscopy at 259 nm using a molar extinction coefficient of 15400 M^{-1} cm^{-1}.

Mutagenesis, Expression, and Purification of BirA Variants. Mutations in the BirA coding sequence were generated by oligonucleotide-directed mutagenesis using a pBtac2 (Boehringer Mannheim) plasmid derivative that carries the C-terminally $(His)_6$-tagged $BirA^{wt}$ coding sequence. Polymerase chain reactions were performed using either Pfu Ultra (Agilent) or KOD (Millipore-Sigma) DNA polymerase, and mutations were verified by sequencing the entire coding sequence (ACGT Inc.).

Each BirA variant was expressed in *E. coli* strain HMS174/pMS421 transformed with the appropriate pBtac2BirA-His derivative plasmid.[21] The variant proteins were purified as previously reported,[14] with the exception of the introduction of a Q-sepharose chromatography step prior to final chromatography on SP-sepharose. Protein concentrations were determined by absorption spectroscopy at 280 nm using a molar extinction coefficient of 47510 M^{-1} cm^{-1} calculated from the amino acid composition.[22] The protein purity was estimated to be >95% based on sodium dodecyl sulfate−polyacrylamide gel electrophoresis analysis.[23]

Isothermal Titration Calorimetry (ITC). All titrations were carried out using a VP-ITC calorimeter (Malvern) equipped with a 1.44 mL cell. Proteins were prepared for titration by exhaustive dialysis against binding buffer, removal of any resulting precipitate by filtration [0.22 μm PES syringe filter (SIMSII)], and concentration determination by UV absorbance at 280 nm. Bio-5′-AMP binding measurements were carried out in standard buffer, and proton linkage measurements were performed in standard buffer in which Tris was replaced with 10 mM Bistris, Citrate, or MES. The ligand stock and concentrated protein were diluted into dialysis buffer to the working concentrations immediately before titrations.

Titrations designed to obtain only molar binding enthalpies were carried out under conditions of total association at partial saturation (TAPS),[24] in which the ligand quantitatively binds to the protein in the first few injections. For each measurement, the sample cell contained a BirA variant at a concentration of 2−5 μM and the injection syringe was filled with a 20−50 μM ligand solution. A total of 14 injections were made, including an initial 2 μL injection, followed by 6 × 13 μL injections, each of which provides the heat of ligand binding and ligand dilution. After the protein had been saturated with a 120 μL ligand injection, 6 × 13 μL injections were performed to obtain the ligand dilution heat. The net ligand binding heat was obtained by subtracting the ligand dilution heat from the heat of the six initial ligand injections.

Equilibrium binding titrations were carried out using the direct or displacement method. In direct titrations, a bio-5′-AMP solution at a concentration of 5−20 μM was titrated into the sample cell containing the BirA variant at 0.5−2 μM. The titrations were initiated with a 2 μL injection, followed by other 17 × 16 μL injections.[7] In displacement (competitive) titrations, one 2 μL plus 22 × 13 μL volumes of a bio-5′-AMP solution were injected into a biotin-saturated BirA solution. The reported binding parameters were based on at least two independent titrations, with the majority representing at least three.

Sedimentation Equilibrium Measurements. HoloBirA dimerization was measured by sedimentation equilibrium in standard buffer at 20 °C using an Optima XL-I analytical ultracentrifuge equipped with a four-hole An-60 Ti rotor

https://dx.doi.org/10.1021/acs.biochem.9b01006
Biochemistry 2020, 59, 790−801

(Beckman Coulter). To ensure saturation, bio-5′-AMP was added to protein at a 1.5:1 molar ratio under stoichiometric conditions. Samples containing 60, 50, and 40 μM holoBirA monomer were loaded into standard 12 mm six-channel cells and centrifuged at 18000, 21000, and 24000 rpm, respectively. After centrifugation for 8 and 9 h at each speed, absorbance scans (step size of 0.001 mm, five averages) were acquired at 300 nm. Overlays of the two scans indicated that the system had reached equilibrium. At least two independent measurements of the equilibrium dimerization constant were performed for each variant.

Data Analysis. ITC data were analyzed using the Microcal software suite in Origin 7.0. The heat of ligand dilution, which was calculated from the average of the heats of the final three to five injections, was subtracted from each raw injection heat. Injection heats were then normalized to molar enthalpy, and the resulting isotherm was analyzed using a single-site binding model for direct titrations and the competitive binding model for displacement titrations.

Sedimentation equilibrium data were analyzed using Nonlin[25] in Heteroanalysis version 1.1.0.58 (https://core.uconn.edu/resources/biophysics#au-software). The equilibrium dissociation constant (K_D) for dimerization was obtained by global nonlinear least-squares analysis of nine data sets using a monomer−dimer model:

$$c(r) = \delta + c(r_o)e^{\sigma_m(\frac{r^2-r_o^2}{2})} + K_A[c(r_o)]^2 e^{2\sigma_m(\frac{r^2-r_o^2}{2})} \quad (1)$$

where $c(r)$ is the protein concentration at position r, $c(r_o)$ is the protein concentration at reference radial position r_o, K_A is the equilibrium association constant governing dimerization, δ is the baseline offset, and σ_m is the reduced molecular weight for the BirA monomer calculated using the equation

$$\sigma_m = \frac{M(1-\bar{\nu}\rho)}{RT}\omega^2 \quad (2)$$

where M is the His-tagged BirA monomer molecular weight of 36100 g/mol, $\bar{\nu}$ is the partial specific volume that was experimentally determined to be 0.755 cm^3/g,[8] ρ is the buffer density calculated using Sednterp version 1.09, ω is the angular velocity of the rotor, and RT is the gas constant times temperature (kelvin).

Molecular Dynamics Simulations and Analysis. MD simulations were performed on BirA, both the wild type (wt) and its variants, in complex with the co-repressor analogue biotinol-5′-AMP (btnOH-AMP), with chain A of the BirA dimer structure in Protein Data Bank (PDB) entry 2EWN[13] used as the starting configuration of the complex. The simulation trajectories used in this study were taken from our previous publication.[17] The GROMACS 4.6 simulator[26−28] with the OPLS-AA force field[29] was used for simulation. For each simulation, the protein was placed in a rhombic dodecahedral box with boundaries extending out ∼1 nm from the protein. The system was then solvated with ∼20300 SPC/E water molecules.[30] Random replacement of a water molecule with a Na^+ counterion rendered the system neutral. The duration of the production run, using an *NPT* ensemble at 300 K and 1 atm, was 1 μs, with the final 500 ns used in trajectory analysis. Additional details of the simulation setup are provided in the Supporting Information.

A BirA residue network was calculated using a method based on Ribeiro and Ortiz[31] in which communication between residue pairs is assumed to be transmitted along minimum energy paths.[31] To calculate the shortest (low-energy) paths, a residue network was first constructed on the basis of the MD simulation, with the final 500 ns of the simulation trajectory used for analysis. In the network, each protein residue is considered a node and connections between a pair of nodes (residues) by an edge required contact for at least 20% of the analyzed simulation time. Contacts were identified using a distance-based cutoff, with distances between all pairs of atoms in the residues considered. The distance cutoff for each pair of atoms was 1.7 times the sum of their van der Waals radii. Use of this criterion allowed capture of both secondary and tertiary features of the BirA protein structure. For each residue i, edges with residues $i \pm 1$, $i \pm 2$, and $i \pm 3$ were excluded. The weight (or length), ω_{ij}, of each edge in the network was calculated using the pairwise interaction energy, ε_{ij}, between residues i and j connected by that edge. This pairwise interaction energy was defined as the sum of all nonbonded interactions between the residues and was calculated at each time step. The weight, ω_{ij}, was calculated from ε_{ij} as follows:

$$\omega_{ij} = \varepsilon_{ij}^{-1/3} \quad (3)$$

This functional form of the edge weight gives similar weight to both hydrogen bonds and salt bridges.

The shortest paths between all nonlocal residue pairs were calculated for trajectory frames sampled at 80 ps intervals using the Floyd−Warshal algorithm[32] to generate an ensemble of shortest paths between all nonlocal residue pairs. Residues i and j are defined as nonlocal if they are separated by more than three residues in the protein sequence. Residues most likely to contribute to the network were defined by their betweenness centrality, C_B, which provides a measure of the influence of a node in a network by computing the extent of its participation in the shortest paths between nodes. The normalized betweenness centrality for node v is calculated as

$$C_B(v) = \frac{\sum_{p\neq q\neq v\in V} \sigma(p, q, v)}{\max(\sum_{p\neq q\neq v\in V} \sigma(p, q, v))} \quad (4)$$

where $\sigma(p, q, v)$ is the shortest path between nodes p and q that passes through node v and V is the set of nodes.

In the network calculations, the final 500 ns of the entire trajectory was divided into 10 sets, with each set spanning an approximately 45 ns window. This window size avoided the serial correlation observed in the punctual stress autocorrelation analysis (see below). The betweenness centrality of a particular residue was calculated for each set and normalized to the residue with the largest C_B value. After the centrality measures had been generated for each set, the values were averaged across all 10 sets. Errors in the resulting betweenness centrality for each residue reflect the standard deviation of the averaged betweenness centrality values calculated for all 10 sets.

The force distribution analysis, based on the method outlined by Stacklies et al.[33] and Costescu and Grater,[34] was carried out for wild type and variant holoBirA species. Residue pairwise forces, which are based on bonded and nonbonded interactions, were used to calculate the punctual stress using the time-resolved force distribution analysis (TRFDA) code. These calculations were carried out on re-runs of the final 500 ns of each MD trajectory. The punctual stress for each residue i

https://dx.doi.org/10.1021/acs.biochem.9b01006
Biochemistry 2020, 59, 790−801

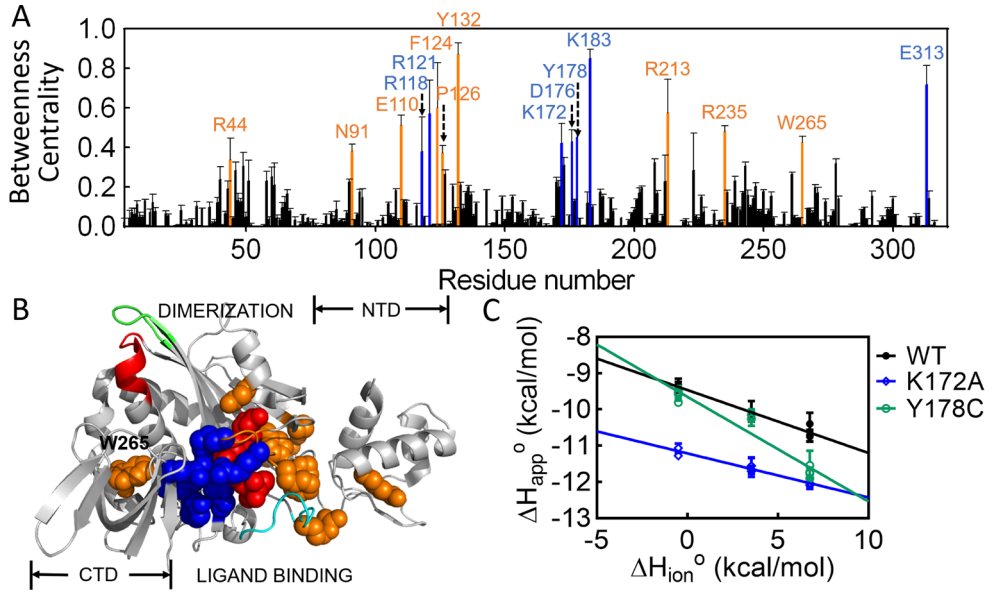

Figure 2. Computationally determined residue network in holoBirA. (A) Betweenness centrality values for each residue with error bars representing the standard deviation obtained from 50 sets of averaged probabilities. (B) Positions of high-likelihood network residues on the holoBirA structure. Color code for panels A and B: red, btnOH-AMP ligand; blue, network residues observed in both the structure and the computation; orange, residues identified solely from computation. (C) Proton release is linked to effector binding. Solid lines result from linear regression using eq 1 with error bars representing the 67% confidence intervals.

is the sum of the absolute values of pairwise forces exerted by all other residues j on that residue.

$$S_i = \sum_{j,i\neq j} |F_{ij}| \tag{5}$$

This calculation generates the punctual stress for each of the 317 residues that were modeled in the structure for every frame, which is then averaged across all frames. Initial analysis of the punctual stress for each residue spanning the final 500 ns of the simulation trajectory indicated an autocorrelation between residues E313 and K172, with a coefficient that dropped below 0.2 at intervals greater than ~20 ns. This correlation was avoided in the averaging by dividing the final 500 ns of the trajectory into 10 sets, with each set spanning ~45 ns. The final punctual stress value for each residue, which represents the average value for the 10 sets, was used to calculate the per residue punctual stress difference between each variant and the wt protein. The statistical significance of each punctual stress difference was evaluated using a two-sample t test ($p < 0.01$). For each residue, the error in the absolute punctual stress difference was calculated as the sum of the standard deviations of the averaged per residue punctual stress obtained for the 10 sets.

Volume calculations were obtained for the helical segments defined by residues 146−160, 234−257, and 260−270, which were selected on the basis of the secondary structure assignments in PDB entry 2EWN and visual inspection of the protein structure. The total volume occupied by these segments in each BirA variant was obtained using the convex hull algorithm implemented in Python 2.7, where the Cα atoms in the helical regions defined the points in the hull.[35] Water molecules within the tessellated space of the convex hull, which was generated using the Delaunay triangulation algorithm, were defined by the presence of oxygen atoms. Both volume and water occupancy for the variants were obtained as probability distributions by calculating the values for multiple frames in the final 500 ns of each MD trajectory.

RESULTS

Computational Analysis Reveals an Extensive Residue Network in HoloBirA. The residue network previously identified in holoBirA^{wt} was based on visual inspection of the structure, an inherently biased process. Consequently, an alternative energy-based analysis was used to identify residue networks in BirA. Computational network analysis of equilibrium trajectories from all-atom MD simulations was performed using a method in which holoBirA residues and the ligand are ranked according to the frequency with which each participates in pairwise low-energy (favorable) paths with nonlocal nodes, amino acid residues or the ligand, in the protein.[31,36] The analysis was performed on the holoBirA monomer, the allosterically activated species for dimerization, with the goal of identifying residues that may function in coupling between the distant disorder-to-order transitions on the effector binding and dimerization surfaces.

The computational analysis yields a more extensive network that, nonetheless, includes the majority of the residues identified by visual inspection (Figure 2A). The 317 amino acid residues and the ligand included in the analysis were ranked according to the magnitudes of their "betweenness centrality", and those in the top 5%, 16 amino acid residues and the effector, were designated as high-probability nodes. For the remainder of the paper, the network refers to these residues, which comprise a nearly continuous surface on one face of the protein that extends from the N-terminal domain−central domain interface to the interface formed between the central and C-terminal domain (Figure 2B).

On the basis of their relationships to effector binding and the disorder-to-order transitions on the ligand binding surface, the network can be divided into two residue subsets. One subset, in which the majority of the residues have charged side

https://dx.doi.org/10.1021/acs.biochem.9b01006
Biochemistry 2020, 59, 790−801

chains, includes the effector and seven of the eight amino acids previously identified from the holoBirA structure (Figure 2A). Consistent with its central role in allosteric activation, the effector is by far the highest-ranking node in the network (Figure S1). Most of the residues in this first subset either form direct electrostatic bonding interactions with the phosphate group on the effector or contribute to a second shell of electrostatic interactions. These residues also connect the central domain to the C-terminal domain via residue E313. The second network subset, which includes E110, F124, P126, Y132, R213, and R235, is comprised of residues that either fold around the ligand or facilitate folding on the ligand binding surface but do not directly interact with the effector. Residues F124 and P126, which contribute to a hydrophobic cluster that packs on the adenine moiety of the effector, function in both bio-5′-AMP binding and effector-linked dimerization.[14,15] *In vivo* measurements have implicated R235 in BirA-mediated transcription repression.[37−39] In addition to the two residue subgroups, the network residue W265, which does not directly interact with any other highly ranked residues, is unique in its proximity to the dimerization surface. The side chain of this residue packs against the α-helix (residues 145−164 in apoBirA) that is extended upon effector binding to include residues 142−144 (Figure 1). Thus, distinct from the limited structurally defined network, the computationally defined network has connections to disorder-to-order transitions on both BirA functional surfaces. The interactions identified in the network analysis have some probability of forming in the absence of the effector. However, given the central role of the ligand in the network and the contribution of residues from protein segments that are disordered in apoBirA, this probability is likely low for many of the interactions.

ITC Measurements of Proton Linkage Are Consistent with Network Formation in Solution. Both the computation and the structures predict that bio-5′-AMP binding drives formation of the residue network. However, evidence from solution-based measurements is lacking. Because the predicted network includes many electrostatic interactions (Figure 2), its formation should be linked to the release of protons from or the uptake of protons by the protein, which is readily detected using isothermal titration calorimetry (ITC).[40] For example, if as expected with network formation, ligand binding is accompanied by proton release, the heat signal measured via ITC should reflect the sum of the ligand binding heat and the heat of buffer protonation. Measurement of the apparent heat of binding in buffers characterized by a range of ionization enthalpies yields data that adhere to the following relationship:

$$\Delta H^{\circ}_{app} = n_{H^+}\Delta H^{\circ}_{ion} + \Delta H^{\circ}_{int} \quad (6)$$

where ΔH°_{app} is the measured molar heat of binding, ΔH°_{int} is the intrinsic binding enthalpy, and ΔH°_{ion} is the buffer ionization enthalpy. Linear regression of the dependence of ΔH°_{app} on ΔH°_{ion} yields n_{H^+}, the number of protons released ($n_{H^+} < 0$) from or absorbed ($n_{H^+} > 0$) by the protein upon ligand binding.

ITC measurements, which were carried out using the TAPS method, in which ligand quantitatively binds to the protein in each injection, indicate that binding of the effector to BirA is accompanied by proton release. Measurements were carried out at pH 6.0 to enhance protonation of acidic side chains on the protein. Additionally, by using the relatively weak allosteric activator, btnOH-AMP,[41] for the measurements, the contribution of the BirA dimerization heat to the measured enthalpy for the wild type protein was negligible. Consistent with network formation, binding of btnOH-AMP to $BirA^{wt}$ is linked to proton release (Figure 2C and Table S1). Moreover, proton linkage is altered for variants with amino acid substitutions at residue K172 or Y178, each of which is predicted to contribute to the network (Figures 1B and 2A and Table S1). Although these experiments do not enable identification of specific residues that are deprotonated upon effector binding, particularly in a system in which multiple negatively charged groups contribute to the linkage, the net proton release supports network formation.

The Network Residues Function in Effector Binding. Although the proton linkage analysis is consistent with network formation in solution, its functional significance of the network for allostery is not known. Allosteric effector binding activates the BirA monomer for homodimerization. The contributions of a subset of the network residues to this binding/activation process were assessed by measuring the binding of bio-5′-AMP to eight BirA variants with substitutions at network positions using ITC. To avoid a significant contribution of dimerization to the measured heats, all titrations were performed at low protein concentrations relative to those required for self-association. Circular dichroism spectra indicated that the secondary structures of all eight variant proteins are indistinguishable from that of $BirA^{wt}$ (Figure S2). For variants with alanine substitutions at R118, K183, and E313, both the equilibrium constants and the binding enthalpies were obtained from standard titrations, in which bio-5′-AMP is injected into a solution containing apoBirA. Representative data obtained for $BirA^{R118A}$ reveal that the binding is described well by a single-site model and that the binding free energy is 2.2 ± 0.2 kcal/mol less favorable than that measured for $BirA^{wt}$ (Figure 3A and Table 1). Binding of bio-5′-AMP to $BirA^{wt}$ and $BirA^{R121A}$ occurs in the picomolar concentration range, and consequently, the displacement method, in which addition of bio-5′-AMP competes the weaker binding biotin off the protein, was used for these two variants[42,43] (Figure S3 and Table 1). Although bio-5′-AMP also binds very tightly to variants $BirA^{K172A}$ and $BirA^{D176A}$, the heat signals in displacement titrations were too small to obtain reliable data. Consequently, the direct titration method was used for these variants (Figure S3). Because the *c* values, the products of the equilibrium constants and the protein concentrations, employed for these titrations were large (>1000), the reported equilibrium constants should be considered upper limits. Accurate bio-5′-AMP binding enthalpies for all of the tight binding variants were obtained using the TAPS method.

Analysis of the binding titrations performed for all of the variants reveals that network residues contribute significantly to bio-5′-AMP binding. Alanine substitutions of residues R118, R119, K183, and E313 have impacts ranging from +2 to +4 kcal/mol on the binding free energy. Even for variants that bind to bio-5′-AMP with free energies similar to that measured for $BirA^{wt}$, the enthalpic and/or the entropic contribution to the binding process is altered (Figure 3B, Figure S3, and Table 1).

Function of the Network in BirA Allosteric Output, HoloBirA Dimerization. Previously published results indicate that BirA variants with substitutions at network residues Y178 and K172 dimerize less tightly than the wild type protein (Figure 3D and Table 2).[16,19] The contributions of six additional network residues in allosteric output, holoBirA

https://dx.doi.org/10.1021/acs.biochem.9b01006
Biochemistry 2020, 59, 790−801

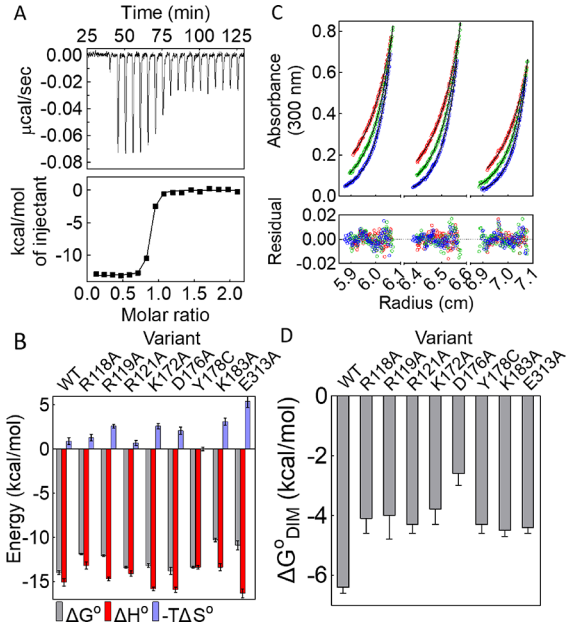

Figure 3. Network residues function in allosteric input and output. (A) Titration of BirA^{R118A} with bio-5′-AMP (top) with analysis of the resulting data using a single-site binding model (bottom). (B) Histograms showing thermodynamics of bio-5′-AMP binding, with error bars representing one standard deviation or the propagated error calculated from at least two independent measurements. (C) HoloBirA^{R121A} sedimentation equilibrium measurement performed at 18K (red), 21K (green), and 24K (blue) rpm with protein samples prepared at 60 μM (left), 50 μM (middle), and 40 μM (right) protein. The top panel shows the absorbance vs radius profiles with best fits to a monomer−dimer model shown as solid lines. The bottom panel shows residuals of the fit. (D) Dimerization free energies for network variants obtained from at least two independent measurements with error bars representing the 67% confidence intervals.

dimerization,[44] were assessed by measuring the dimerization free energies of the variants in their bio-5′-AMP-bound forms using sedimentation equilibrium. For each variant, the measurements were performed at three rotor speeds on protein samples prepared at three concentrations and the nine resulting data sets were globally analyzed using a monomer−dimer model. Results obtained for holoBirA^{R121A}, which indicate excellent agreement between the data and the model, yield an equilibrium dimerization constant of (7 ± 2) × 10^{-4} M, 40-fold weaker than that measured for holoBirA^{wt} (Figure 3C). Notably, with this weak dimerization the maximal fraction dimer at the highest holoBirA concentration is relatively low, at 8.9% of the total monomer concentration. Nevertheless, analysis of the data using a single-species model yielded an average molecular weight of 42 ± 1 kDa, higher than the value of 36 kDa expected for the monomer. Moreover, the square root of the variance value associated with a monomer−dimer fit was smaller than that obtained using a single-species model. Results of sedimentation equilibrium measurements performed on all variants with network residue substitutions indicate dimerization that is significantly weaker than that measured for holoBirA^{wt}, with Gibbs free energy penalties ranging from 2 to 4 kcal/mol (Figure 3D, Figure S4, and Table 2).

Table 2. BirA Variant Dimerization Energetics[a]

variant	K_D (M)	$\Delta G°$ (kcal/mol)
wt	(1.6 ± 0.5) × 10^{-5}	−6.4 ± 0.2
R118A	(1.0 ± 0.6) × 10^{-3}	−4.1 ± 0.5
R119A	(1.1 ± 0.8) × 10^{-3}	−4.0 ± 0.8
R121A	(6 ± 2) × 10^{-4}	−4.3 ± 0.3
K172A[b]	(1.4 ± 0.8) × 10^{-3}	−3.8 ± 0.5
D176A[b]	(1 ± 1) × 10^{-2}	−2.6 ± 0.4
Y178C[c]	(7 ± 3) × 10^{-4}	−4.3 ± 0.3
K183A	(4 ± 1) × 10^{-4}	−4.5 ± 0.2
E313A	(5 ± 2) × 10^{-4}	−4.4 ± 0.2

[a]All measurements were carried out in standard buffer at 20 °C. Errors were propagated from those obtained from at two independent measurements. The Gibbs free energies of dimerization were calculated using the equation $\Delta G° = RT \ln K_D$. [b]Value previously reported in ref 16. [c]Value previously reported in ref 19.

Force Distribution Analysis Indicates Coupling between Disorder-to-Order Transitions and the Network in BirA Allostery. The relationship of the residue network to the distant disorder-to-order transitions that function in BirA allostery was investigated using force distribution analysis (FDA), a method in which one calculates the mechanical, or punctual, stress experienced by each amino acid residue in a protein from all pairwise residue forces. Thus, the method provides information about the energy distribution in a protein. If the network functions in coupling the distant transitions on the dimerization and ligand binding surfaces, the transitions should be accompanied by changes in the force experienced by network residues. Furthermore, perturbation of

Table 1. BirA Variant Bio-5′-AMP Binding Thermodynamics[a]

protein	K_D (M)	$\Delta G°$ (kcal/mol)	$\Delta H°$ (kcal/mol)	$-T\Delta S°$ (kcal/mol)	n
wt[b,c]	(4 ± 1) × 10^{-11}	−14.0 ± 0.2	−15.1 ± 0.4	0.9 ± 0.4	0.88 ± 0.02
R118A[d]	(1.3 ± 0.3) × 10^{-9}	−11.9 ± 0.1	−13.2 ± 0.4	1.3 ± 0.4	0.88 ± 0.06
R119A[c]	(9 ± 2) × 10^{-10}	−12.1 ± 0.1	−14.7 ± 0.2	2.6 ± 0.2	0.83 ± 0.02
R121A[b,c]	(1.0 ± 0.2) × 10^{-10}	−13.4 ± 0.1	−14.1 ± 0.3	0.7 ± 0.3	0.94 ± 0.05
K172A[c]	(1.5 ± 0.4) × 10^{-10}	−13.2 ± 0.2	−15.8 ± 0.2	2.6 ± 0.3	0.90 ± 0.01
D176A[c]	(5 ± 6) × 10^{-11}	−13.8 ± 0.4	−15.9 ± 0.3	2.1 ± 0.4	0.86 ± 0.02
Y178C[b,c]	(1.0 ± 0.2) × 10^{-10}	−13.4 ± 0.1	−13.4 ± 0.2	0 ± 0.2	1.0 ± 0.1
K183A[d]	(2.2 ± 0.6) × 10^{-8}	−10.3 ± 0.2	−13.4 ± 0.4	3.1 ± 0.4	0.83 ± 0.02
E313A[d]	(1 ± 0.9) × 10^{-8}	−10.9 ± 0.5	−16.3 ± 0.5	5.4 ± 0.7	0.79 ± 0.03

[a]Measurements were carried out in standard buffer at 20 °C. The reported errors represent the larger of either the standard deviation or the propagated error obtained from at least two independent measurements. The Gibbs free energies and entropic contributions were calculated using the equations $\Delta G° = RT \ln K_D$ and $\Delta G° = \Delta H° - T\Delta S°$, respectively. [b]Equilibrium constants obtained from displacement tirations. [c]Binding enthalpies obtained from TAPS. [d]Binding enthalpies obtained from equilibrium titrations.

https://dx.doi.org/10.1021/acs.biochem.9b01006
Biochemistry 2020, 59, 790−801

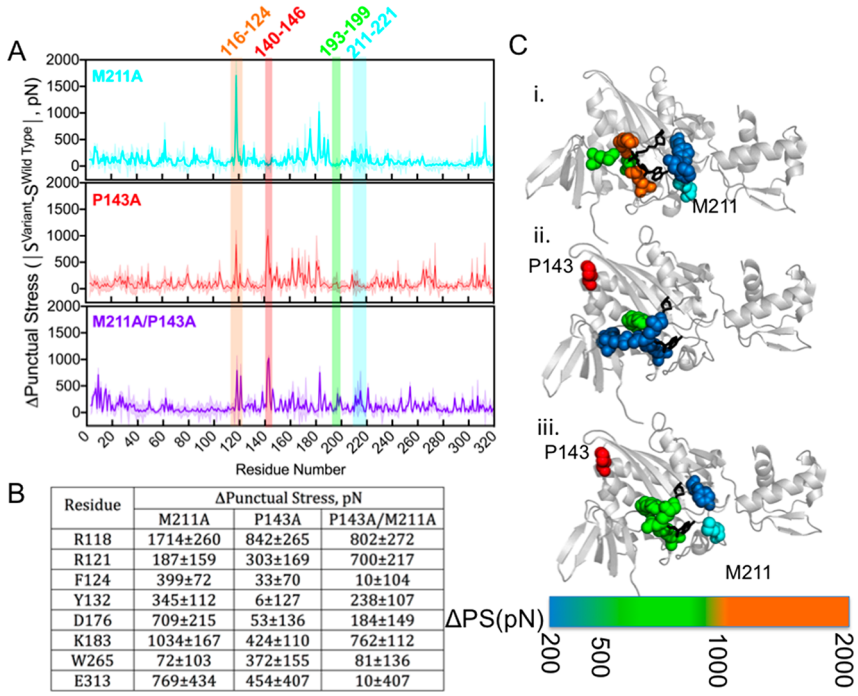

B

Residue	ΔPunctual Stress, pN		
	M211A	P143A	P143A/M211A
R118	1714±260	842±265	802±272
R121	187±159	303±169	700±217
F124	399±72	33±70	10±104
Y132	345±112	6±127	238±107
D176	709±215	53±136	184±149
K183	1034±167	424±110	762±112
W265	72±103	372±155	81±136
E313	769±434	454±407	10±407

Figure 4. Force distribution analysis reveals coupling between the network and disorder-to-order transitions. (A) Per residue absolute punctual stress difference for each holoBirA variant with respect to holoBirA wt. (B) Numerical values of punctual stress differences at network residue positions for the three variants. (C) HoloBirA structural model showing network positions with significant punctual stress differences in (i) $BirA^{M211A}$, (ii) $BirA^{P143A}$, and (iii) $BirA^{P143A/M211A}$. The color scale for the magnitude of the punctual stress difference, ΔPS, is shown on the bar.

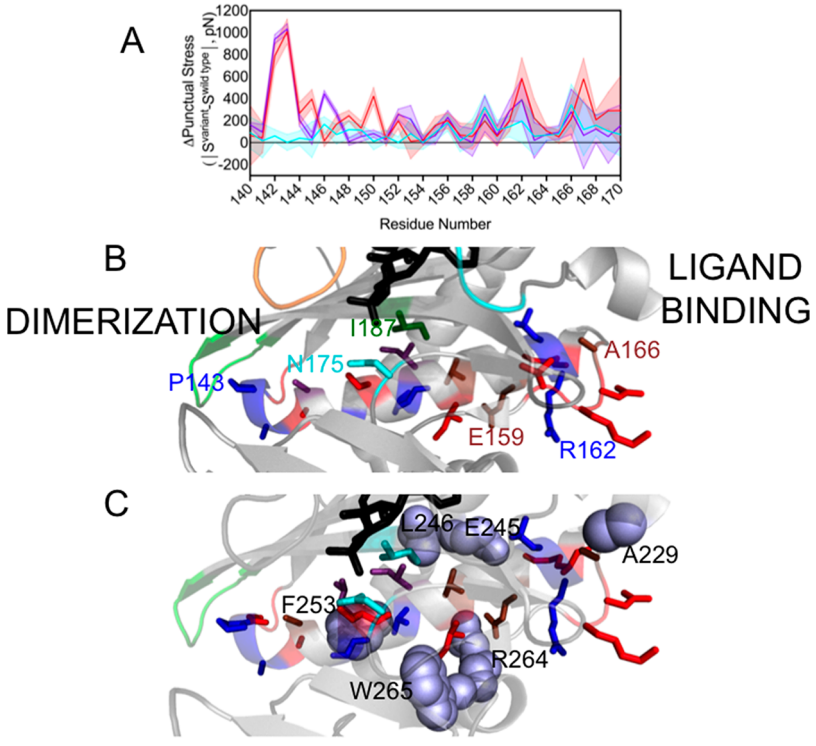

Figure 5. Changes in punctual stress are observed in an α-helix that functions in holoBirA dimerization and the loop C-terminal to it. (A) Punctual stress differences observed for residues in holoBirA helix 142−164 and the C-terminal segment 165−169: $holoBirA^{M211A}$, cyan; $holoBirA^{P143A}$, red; $holoBirA^{P143A/M211A}$, purple. The shaded region represents the standard error in the punctual stress difference. (B) Residue locations of punctual stress changes shown on the helix and loop with colors indicating variants in which punctual stress values differ from those found in $holoBirA^{wt}$: red, P143A; blue, P143A and P143A/M211A; brown, M211A, P143A, and M211A/P143A; cyan, M211A (residue N175); green, M211A and P143A (residue I187). Numbering is provided at select residue positions to orient the reader. (C) Residues (lavender spheres) in $holoBirA^{wt}$ that form nonbonded interactions with dimerization helix and C-terminal extension residues and undergo changes in punctual stress in the variants.

https://dx.doi.org/10.1021/acs.biochem.9b01006
Biochemistry 2020, 59, 790−801

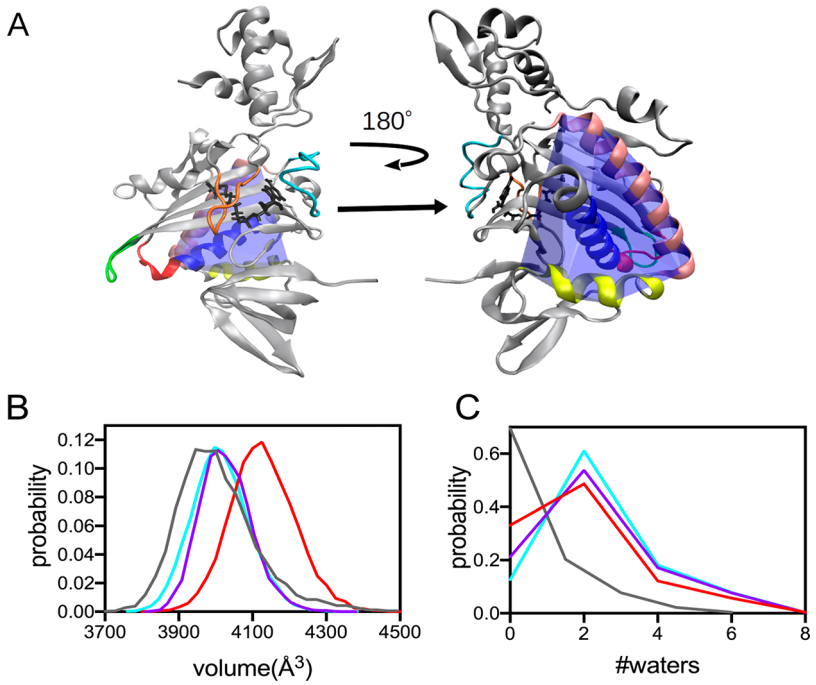

Figure 6. Helix packing is altered in the BirA variants. (A) Model of the holoBirA monomer structure with the convex hull (blue) defined by helices comprised of residues 146−160 (royal blue), 234−257 (tan), and 260−270 (yellow) highlighted. The coloring of the loop regions is identical to that used in Figure 1. (B and C) Distributions of volumes and water count probability, respectively, calculated for the convex hull defined by the helices in panel A for holoBirA^{wt} (gray) and variants with substitutions M211A (cyan), P143A (red), and P143A/M211A (purple).

the transitions is expected to alter the punctual stress experienced by network residues. Force distribution analysis of BirA variants in which the disorder-to-order transitions are disrupted was performed to test this prediction. The holo forms of BirA^{wt} and its variants with alanine substitutions at P143, M211, and both P143 and M211 (Figure 4) were subjected to the analysis. Previous studies indicated that single-alanine substitutions of residues P143 and M211, which perturb the disorder-to-order transitions at the dimerization and ligand binding surfaces, respectively, alter effector binding and/or effector-linked dimerization (Table S2).[15−17] In the double variant, BirA$^{P143A/M211A}$, favorable energetic coupling in effector binding is observed between the two residues (Table S2). Thus, these variants provide ideal tools for investigating the relationship between disorder to order on the two allosterically linked functional surfaces and the network in BirA.

FDA indicates that perturbations to disorder-to-order transitions are accompanied by changes in the stress experienced by network residues. Moreover, the residue locations and magnitudes of these changes vary with the amino acid substitution. The analysis was carried out on the equilibrium portion, the final 500 ns, of the MD trajectories obtained for each holo variant, and the results are presented as the difference in punctual stress at each residue in a variant relative to that experienced by the same residue in the wild type protein. For each single-alanine variant, significant punctual stress differences (>300 pN) are observed at the substituted residue position as well as at multiple network residues (Figure 4A−C). For example, holoBirA^{M211A} shows the strongest effects on the stress experienced by network residues R118, D176, K183, and E313. In addition, consistent with its weak binding to bio-5′-AMP, stress alterations are observed at network residues F124 and Y132, which both participate directly in disorder-to-order transitions on the ligand binding surface. For holoBirA^{P143A}, punctual stress perturbations are found at network residues R118, R121, K183, W265, and E313. However, the magnitudes of the stress perturbations for R118, K183, and E313 are significantly lower than those observed in BirA^{M211A}. In the double variant, which shows energetically favorable coupling between the distant P143 and M211 residues[17] in effector binding, the punctual stress perturbations for residues R118, D176, K183, and E313 are much lower than those found in the single variant, M211A, a result consistent with partial reversal of the bio-5′-AMP binding defect exhibited by the single mutant. In fact, the mean value of the punctual stress difference for E313 in the double variant is close to zero. Moreover, no perturbation is observed in the stress at residue F124. Combined, the computational results indicate correlations among perturbations to disorder-to-order transitions, functional effects on allostery, and force distribution in the residue network.

The Variants Show Punctual Stress Changes in an α-Helix That Functions in Dimerization. In addition to the network residues, significant changes to punctual stress are observed at residues in an α-helix that plays a critical role in dimerization and in residues C-terminal to it. On the dimerization surface, bio-5′-AMP binding is accompanied by extension of the helix, which is comprised of residues 147−164 in apoBirA, to incorporate residues 142−146. The M211A, P143A, and M211A/P143A variants are characterized by penalties to dimerization of +1.4, +1.0, and +2.4 kcal/mol, respectively. Consistent with the P143A substitution, which decreases the helicity of residues 142−146, punctual stress differences for residues 142−148 in holoBirA^{P143A} and BirA$^{P143A/M211A}$ (Figure 5A and Table S3) are large. In all three variants, significant stress differences are also found at other helical residues, with the location and magnitudes of the

https://dx.doi.org/10.1021/acs.biochem.9b01006
Biochemistry 2020, 59, 790−801

perturbations varying for the different variants (Figure 5A,B and Table S3). In addition to the perturbations in the helix itself, residues that form nonbonded contacts with helical residues experience punctual stress changes (Figure 5C and Table S3). For example, W265, a network residue that packs against I155 in the helix, shows a large punctual stress difference in holoBirA^{P143A}. In all three variants, the stress experienced by R264, which forms an electrostatic interaction with helix residue E159, is altered. In the 165−169 segment that is C-terminal to the helix, changes are observed at residues A166 and D167, and K168 and V169. In the holoBirA structure, A166 packs against ABL residues A229 and the latter three residues form charged hydrogen bonds through their backbone groups to the side chain of residue R162 in helix 142−164. The FDA results indicate that perturbations of disorder to order on the ligand binding and dimerization surfaces are correlated with effects on the interactions of a critical α-helix with the remainder of the protein.

Altered Packing of the α-Helix in the Variants. In FDA, punctual stress is calculated as the absolute value and, consequently, provides no information about the direction of stress changes. In other words, differences in punctual stress may reflect either increased or decreased forces on residues. Thus, FDA provides no insight into the structural origins of changes in net forces at the helix residues. In the BirA structure, helix 142−165 is wedged between two other helices comprised of residues 234−257 and 260−270 (Figure 6A). In light of the observed perturbations to stress in residues in all three helices, the relationship of the observed punctual stress changes in the variants to the packing of these helices was investigated by performing volume calculations. First, a convex hull that wraps around the three helices was constructed for holoBirA^{wt} and the three variants. Because of the loss of helicity in variants with the P143A substitution, only residues 146−160 of the dimerization helix were included in the constructed hulls (Figure 6A). The hull volumes were then calculated for multiple frames in the trajectories for each variant to obtain a distribution of volumes. The resulting probability distributions indicate that the helices occupy a greater volume in the variants than in holoBirA^{wt} (Figure 6B), with the most probable volume occupied by the three helices in the wild type protein being ∼100−300 Å^3 smaller than in the variants. These volume differences are accompanied by differences in the water occupancy, with the helices in the wild type protein containing less water than the variants (Figure 6C). Interestingly, although the volume occupied by the three helices in holoBirA^{P143A} is largest among the three variants, the water content is similar to that of the other two variants. Thus, the volume and water occupancy calculations suggest tighter packing of the dimerization helix in the wild type than in the variant proteins.

DISCUSSION

Although the significance of disorder for protein allostery is well-documented, how the disorder is incorporated into allosteric mechanism is unknown for most systems. In *E. coli* BirA, coupled disorder-to-order transitions on two distant functional surfaces are critical for activating the protein for dimerization. In this work, combined experimental and computational studies reveal how a residue network functions in linking the folding transitions in allostery.

Computational analysis yields a network that, although more extensive, overlaps with that derived from visual inspection of the structure. Although the network has some probability of forming in apoBirA, effector binding greatly enhances this probability, either because of direct network residue contacts with the effector (R118, R121, K172, and K183) or because many network residues are in segments that fold concomitant with bio-5′-AMP binding. Notably, residues P126 and F124, both of which directly participate in disorder-to-order transitions at the ligand binding site, are among the computationally identified network residues.[14,15] Thus, the hydrophobic packing that accompanies folding on the ligand binding surface enables formation of the electrostatic interactions in the vicinity of the effector molecule. The network also includes one C-terminal domain residue, E313, which forms interactions with multiple residues from the central domain. By contrast, the few identified N-terminal DNA binding domain residues have no connections with other network residues, a result that is consistent with the apparent decoupling of dimerization energetics from the affinity of the resulting holoBirA dimer for DNA observed for a number of BirA variants.[45]

Measurements performed on BirA variants with alanine substitutions at network positions reveal important functional roles for the network in both bio-5′-AMP binding and coupled dimerization. Additionally, previous genetic studies indicated that residue R235 contributes to BirA-mediated transcription repression. Finally, residues P126 and F124 contribute to both effector binding and holoBirA dimerization.[14,15] Only residue R119, which was designated as a network residue on the basis of structure, was not identified in the computational analysis, and experimental measurements reveal its importance for bio-5′-AMP-induced dimerization. Structural data suggest that rather than contributing to allostery, R119 directly contributes to the dimerization interface. Notably, with the exception of R119, the network variants experimentally tested in this work, which uniformly show large perturbations to the dimerization free energy, all have amino acid substitutions distant from the dimerization interface.

The residue network and the disorder-to-order transitions on the ligand binding surface are tightly integrated in BirA allosteric activation. First, residues that directly participate in disorder-to-order transitions, including P126 and F124, contribute to both the network and allostery.[15] Second, as noted above, many network interactions are enabled by the disorder-to-order transitions. Finally, FDA indicates that perturbations of disorder to order in the ligand binding surface are accompanied by changes in the punctual stress experienced by network residues.

The energy-based network alone, in which only one residue, W265, in the vicinity of the dimerization surface is a member, provides little insight into how effector binding is communicated to disorder-to-order transitions on that surface. The combined network and force distribution analysis suggests that enhanced packing of the α-helix that functions in dimerization plays a role in this communication. In the M211A, P143A, and M211A/P143A variants, all of which dimerize less tightly than BirA^{wt}, punctual stress perturbations are observed at multiple residues in the helix as well as in the 165−169 segment C-terminal to the helix. These stress perturbations in the helix are correlated with changes in the stress experienced by residues that interact with the helix (Figure 5C and Table S3) and with the volume occupied by this central helix and its two neighboring helices. Comparison of apo and holoBirA structures indicates that in holoBirA the central helix

https://dx.doi.org/10.1021/acs.biochem.9b01006
Biochemistry 2020, 59, 790−801

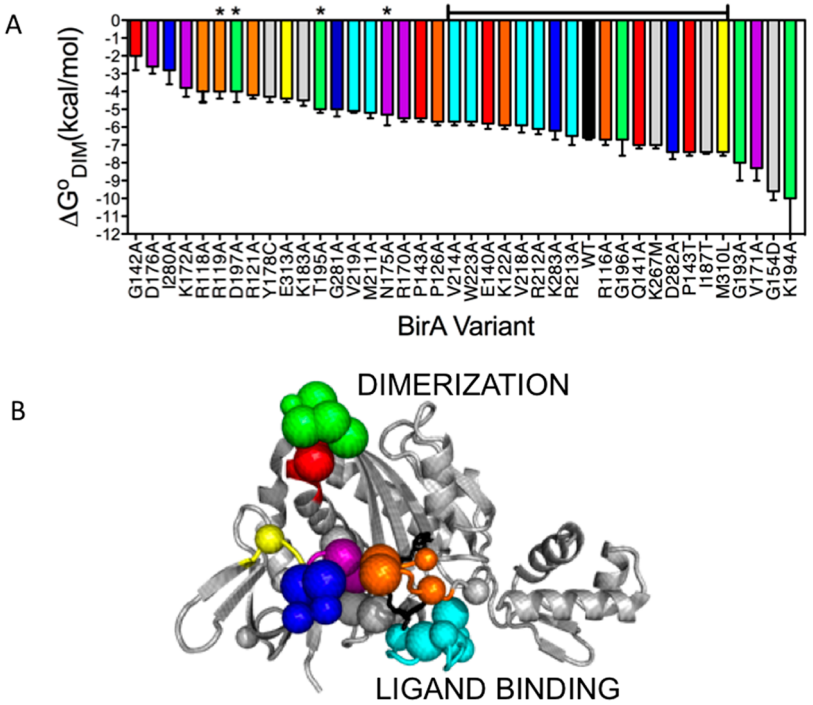

Figure 7. Amino acid substitutions tune the BirA allosteric response. (A) Amino acid substitutions in BirA yield a broad range of holoBirA dimerization free energies. The bracketed line above the bars indicates variants with substitutions that dimerize with free energies within ±1 kcal/mol of that of holoBirA^{wt}, and asterisks signify residues that contribute directly to the dimer interface. (B) Cα atoms of amino acid positions in panel A shown on the holoBirA monomer with small spheres signifying modest (within ±1 kcal/mol) and large spheres indicating larger (>±1 kcal/mol) effects on the dimerization free energy. Color code: loops, orange, 116−124; red, 140−146; purple, 170−176; green, 193−199; cyan, 211−222; blue, 280−283; yellow, 310−313; gray, protein core. The model was created in Pymol with PDB entry 2EWN as input.

interactions fall into two classes. Formation of the first class of interactions is contingent upon effector binding. For example, reorganization of the loop containing residues 170−176 upon bio-5′-AMP binding results in integration of residue D176 into the network and enables hydrogen bonding between N175 and helix residue S150. Additionally, BBL folding upon bio-5′-AMP binding allows R118 and R121 to form network interactions that are coupled to enhanced packing of residue I187 with helix residues I153 and M157. Finally, ABL folding decreases the distance between residue A166 in the loop that is C-terminal to the helix and residue A229 in the ABL from 7.5 Å in apoBirA to 3.7 Å in holoBirA. A second category of dimerization helix interactions that are perturbed in the variants includes a number of nonbonded interactions that are conserved in apo- and holoBirA but differ in distance in the two structures. These include an electrostatic interaction between E159 and R264 and hydrophobic packing between helix residues V156, V152, and V155 and L246, F253, and network residue W265, respectively. The structural data also indicate that ligand binding results in distance changes in charged hydrogen bonds that form among the D167, K168, and V169 backbone carbonyl groups in loop 165−169 with the side chain of helix residue R162. On the basis of changes in punctual stress, many of both classes of helix interactions are altered to varying extents in the variants. These alterations likely form the basis of the looser packing of the dimerization helix with its two neighboring helices in the variants indicated by the volume calculations (Figure 6).

Overall, the combined FDA results and structural data support a role for the network in enhancing packing of the BirA dimerization helix in the central domain of the effector-bound protein. Previously published results support this enhanced packing. First, HDX-MS measurements indicate that effector binding is accompanied by protection of backbone amide groups distributed throughout the protein from deuterium exchange.[46] Second, heat capacity changes associated with bio-5′-AMP binding by BirA variant monomers are linearly correlated with the dimerization free energy of the resulting holo monomer, with smaller negative heat capacity changes associated with weaker dimerization.[47] These thermodynamics are consistent with a decrease in the level of folding/packing in the weakly dimerizing proteins.[48,49] Importantly, none of amino acid substitutions in the variants subjected to experimental studies in that work were at residues that form noncovalent bonds at the dimerization interface. The relationships among helix packing in effector-bound BirA, the overall folding thermodynamics of the protein, and extension of the helix on the dimerization surface are currently under investigation.

BirA allostery reflects contributions from numerous residues distributed throughout the structure (Figure 7). Combined computational and experimental results indicate that residues on both functional surfaces as well as those in the network function in allostery. Additionally, on the basis of the FDA presented in this work, residues that function in packing of helices in the protein core are also predicted to contribute to the allosteric response, a prediction that is currently being experimentally tested. At a biological level, this distributed mechanism renders BirA allostery robust to protein sequence changes. Indeed, amino acid substitutions at 18 different residues result in holoBirA dimerization free energies that are within ±1 kcal/mol of that measured for holoBirA^{wt} (Figure 7). However, in addition to these modest responses, residues in the network, particularly in the electrostatic core, as well as a

https://dx.doi.org/10.1021/acs.biochem.9b01006
Biochemistry 2020, 59, 790−801

subset of residues on the ligand binding and dimerization surfaces are highly sensitive to substitution. Notably, a majority of these residues, including those on the dimerization surface, do not directly contribute to the dimer interface (Figure 7).

Protein disorder is important for the thermodynamic coupling that lies at the heart of allostery,[50] and manipulation of this disorder provides a means of modulating the coupling.[15,16,18,51] The results reported in this work demonstrate that a residue network can work in concert with distant disorder-to-order transitions to effect allostery. The results also support the ensemble view of allostery in which the functional output can be tuned via redistribution of energy at multiple residues in a protein.[52]

■ ASSOCIATED CONTENT

Supporting Information

The Supporting Information is available free of charge at https://pubs.acs.org/doi/10.1021/acs.biochem.9b01006.

MD simulation procedure, three tables, and four figures (PDF)

■ AUTHOR INFORMATION

Corresponding Author

Dorothy Beckett − *Department of Chemistry & Biochemistry, University of Maryland, College Park, Maryland 20742, United States;* orcid.org/0000-0002-7838-0651; Email: dbeckett@umd.edu

Authors

Jingheng Wang − *Department of Chemistry & Biochemistry, University of Maryland, College Park, Maryland 20742, United States*

Riya Samanta − *Biophysics Graduate Program, University of Maryland, College Park, Maryland 20742, United States*

Gregory Custer − *Fischell Department of Bioengineering, University of Maryland, College Park, Maryland 20742, United States;* orcid.org/0000-0002-9752-5748

Christopher Look − *Fischell Department of Bioengineering, University of Maryland, College Park, Maryland 20742, United States*

Silvina Matysiak − *Fischell Department of Bioengineering, University of Maryland, College Park, Maryland 20742, United States;* orcid.org/0000-0003-3824-9787

Complete contact information is available at: https://pubs.acs.org/10.1021/acs.biochem.9b01006

Author Contributions

‖J.W. and R.S. contributed equally to this work.

Funding

This work was supported by National Institutes of Health (NIH) Grant R01-GM129327 (National Institute of General Medical Sciences) and NIH Grant S10 RR15899 to D.B.

Notes

The authors declare no competing financial interest.

■ REFERENCES

(1) Monod, J. (1971) *Chance and Necessity an Essay on the Natural Philosophy of Modern Biology*, translated from the French by Austryn Wainhouse.

(2) Iwata, S., Kamata, K., Yoshida, S., Minowa, T., and Ohta, T. (1994) T and R states in the crystals of bacterial L-lactate dehydrogenase reveal the mechanism for allosteric control. *Nat. Struct. Biol. 1*, 176−185.

(3) Knoflach, F., Mutel, V., Jolidon, S., Kew, J. N., Malherbe, P., Vieira, E., Wichmann, J., and Kemp, J. A. (2001) Positive allosteric modulators of metabotropic glutamate 1 receptor: characterization, mechanism of action, and binding site. *Proc. Natl. Acad. Sci. U. S. A. 98*, 13402−13407.

(4) JACOB, F., and MONOD, J. (1961) Genetic regulatory mechanisms in the synthesis of proteins. *J. Mol. Biol. 3*, 318−356.

(5) Larion, M., Salinas, R. K., Bruschweiler-Li, L., Miller, B. G., and Brüschweiler, R. (2012) Order-disorder transitions govern kinetic cooperativity and allostery of monomeric human glucokinase. *PLoS Biol. 10*, e1001452.

(6) Reichheld, S. E., Yu, Z., and Davidson, A. R. (2009) The induction of folding cooperativity by ligand binding drives the allosteric response of tetracycline repressor. *Proc. Natl. Acad. Sci. U. S. A. 106*, 22263−22268.

(7) Ampapathi, R. S., Creath, A. L., Lou, D. I., Craft, J. W., Blanke, S. R., and Legge, G. B. (2008) Order-disorder-order transitions mediate the activation of cholera toxin. *J. Mol. Biol. 377*, 748−760.

(8) Eisenstein, E., and Beckett, D. (1999) Dimerization of the Escherichia coli biotin repressor: corepressor function in protein assembly. *Biochemistry 38*, 13077−13084.

(9) Abbott, J., and Beckett, D. (1993) Cooperative binding of the Escherichia coli repressor of biotin biosynthesis to the biotin operator sequence. *Biochemistry 32*, 9649−9656.

(10) Streaker, E. D., and Beckett, D. (2003) Coupling of protein assembly and DNA binding: biotin repressor dimerization precedes biotin operator binding. *J. Mol. Biol. 325*, 937−948.

(11) Wilson, K. P., Shewchuk, L. M., Brennan, R. G., Otsuka, A. J., and Matthews, B. W. (1992) Escherichia coli biotin holoenzyme synthetase/bio repressor crystal structure delineates the biotin- and DNA-binding domains. *Proc. Natl. Acad. Sci. U. S. A. 89*, 9257−9261.

(12) Weaver, L. H., Kwon, K., Beckett, D., and Matthews, B. W. (2001) Corepressor-induced organization and assembly of the biotin repressor: a model for allosteric activation of a transcriptional regulator. *Proc. Natl. Acad. Sci. U. S. A. 98*, 6045−6050.

(13) Wood, Z. A., Weaver, L. H., Brown, P. H., Beckett, D., and Matthews, B. W. (2006) Co-repressor induced order and biotin repressor dimerization: a case for divergent followed by convergent evolution. *J. Mol. Biol. 357*, 509−523.

(14) Naganathan, S., and Beckett, D. (2007) Nucleation of an allosteric response via ligand-induced loop folding. *J. Mol. Biol. 373*, 96−111.

(15) Eginton, C., Naganathan, S., and Beckett, D. (2015) Sequence-function relationships in folding upon binding. *Protein Sci. 24*, 200−211.

(16) Adikaram, P. R., and Beckett, D. (2012) Functional versatility of a single protein surface in two protein:protein interactions. *J. Mol. Biol. 419*, 223−233.

(17) Wang, J., Custer, G., Beckett, D., and Matysiak, S. (2017) Long Distance Modulation of Disorder-to-Order Transitions in Protein Allostery. *Biochemistry 56*, 4478−4488.

(18) Eginton, C., Cressman, W. J., Bachas, S., Wade, H., and Beckett, D. (2015) Allosteric coupling via distant disorder-to-order transitions. *J. Mol. Biol. 427*, 1695−1704.

(19) He, C., Custer, G., Wang, J., Matysiak, S., and Beckett, D. (2018) Superrepression through Altered Corepressor-Activated Protein:Protein Interactions. *Biochemistry 57*, 1119−1129.

(20) Lane, M. D., Rominger, K. L., Young, D. L., and Lynen, F. (1964) The Enzymatic Synthesis of Holotranscarboxylase from Apotranscarboxylase and (+)-Biotin. II. Investigation of the Reaction Mechanism. *J. Biol. Chem. 239*, 2865−2871.

(21) Kwon, K., and Beckett, D. (2000) Function of a conserved sequence motif in biotin holoenzyme synthetases. *Protein Sci. 9*, 1530−1539.

(22) Gill, S. C., and von Hippel, P. H. (1989) Calculation of protein extinction coefficients from amino acid sequence data. *Anal. Biochem. 182*, 319−326.

(23) Laemmli, U. K. (1970) Cleavage of structural proteins during the assembly of the head of bacteriophage T4. *Nature 227*, 680−685.
(24) Bains, G., and Freire, E. (1991) Calorimetric determination of cooperative interactions in high affinity binding processes. *Anal. Biochem. 192*, 203−206.
(25) Johnson, M. L., Correia, J. J., Yphantis, D. A., and Halvorson, H. R. (1981) Analysis of data from the analytical ultracentrifuge by nonlinear least-squares techniques. *Biophys. J. 36*, 575−588.
(26) Berendsen, H., van der Spoel, D., and van Drunen, R. (1995) GROMACS - A Message-Passing Parallel Molecular-Dynamics Implementation. *Comput. Phys. Commun. 91*, 43−56.
(27) Lindahl, E., Hess, B., and van der Spoel, D. (2001) GROMACS 3.0: a package for molecular simulation and trajectory analysis. *J. Mol. Model. 7*, 306−317.
(28) Hess, B., Kutzner, C., van der Spoel, D., and Lindahl, E. (2008) GROMACS 4: Algorithms for highly efficient, load-balanced, and scalable molecular simulation. *J. Chem. Theory Comput. 4*, 435−447.
(29) Jorgensen, W., Maxwell, D., and TiradoRives, J. (1996) Development and testing of the OPLS all-atom force field on conformational energetics and properties of organic liquids. *J. Am. Chem. Soc. 118*, 11225−11236.
(30) Berendsen, H., Grigera, J., and Straatsma, T. (1987) The missing term in effective pair potentials. *J. Phys. Chem. 91*, 6269−6271.
(31) Ribeiro, A. A., and Ortiz, V. (2014) Determination of Signaling Pathways in Proteins through Network Theory: Importance of the Topology. *J. Chem. Theory Comput. 10*, 1762−1769.
(32) FLOYD, R. (1962) ALGORITHM-97 - SHORTEST PATH. *Commun. ACM 5*, 345−345.
(33) Stacklies, W., Seifert, C., and Graeter, F. (2011) Implementation of force distribution analysis for molecular dynamics simulations. *BMC Bioinf. 12*, 101−105.
(34) Costescu, B., and Grater, F. (2013) Time-resolved force distribution analysis. *BMC Biophys. 6*, 5−9.
(35) Barber, C. B., Dobkin, D. P., and Huhdanpaa, H. T. (1996) The Quickhull algorithm for convex hulls. *ACM Trans. on Mathematical Software 22*, 469−483.
(36) Ribeiro, A. A., and Ortiz, V. (2015) Energy propagation and network energetic coupling in proteins. *J. Phys. Chem. B 119*, 1835−1846.
(37) Barker, D. F., and Campbell, A. M. (1980) Use of Bio-Lac Fusion Strains to Study Regulation of Biotin Biosynthesis in Escherichia-Coli. *J. Bacteriol. 143*, 789−800.
(38) Barker, D. F., and Campbell, A. M. (1981) Genetic and biochemical characterization of the birA gene and its product: evidence for a direct role of biotin holoenzyme synthetase in repression of the biotin operon in Escherichia coli. *J. Mol. Biol. 146*, 469−492.
(39) Buoncristiani, M. R., Howard, P. K., and Otsuka, A. J. (1986) DNA-binding and enzymatic domains of the bifunctional biotin operon repressor (BirA) of Escherichia coli. *Gene 44*, 255−261.
(40) Baker, B. M., and Murphy, K. P. (1996) Evaluation of linked protonation effects in protein binding reactions using isothermal titration calorimetry. *Biophys. J. 71*, 2049−2055.
(41) Brown, P. H., Cronan, J. E., Grotli, M., and Beckett, D. (2004) The biotin repressor: modulation of allostery by corepressor analogs. *J. Mol. Biol. 337*, 857−869.
(42) Sigurskjold, B. W. (2000) Exact analysis of competition ligand binding by displacement isothermal titration calorimetry. *Anal. Biochem. 277*, 260−266.
(43) Brown, P. H., and Beckett, D. (2005) Use of binding enthalpy to drive an allosteric transition. *Biochemistry 44*, 3112−3121.
(44) Streaker, E. D., Gupta, A., and Beckett, D. (2002) The biotin repressor: thermodynamic coupling of corepressor binding, protein assembly, and sequence-specific DNA binding. *Biochemistry 41*, 14263−14271.
(45) Adikaram, P. R., and Beckett, D. (2013) Protein:protein interactions in control of a transcriptional switch. *J. Mol. Biol. 425*, 4584−4594.
(46) Laine, O., Streaker, E. D., Nabavi, M., Fenselau, C. C., and Beckett, D. (2008) Allosteric signaling in the biotin repressor occurs via local folding coupled to global dampening of protein dynamics. *J. Mol. Biol. 381*, 89−101.
(47) Cressman, W. J., and Beckett, D. (2016) Heat Capacity Changes and Disorder-to-Order Transitions in Allosteric Activation. *Biochemistry 55*, 243−252.
(48) Sturtevant, J. M. (1977) Heat capacity and entropy changes in processes involving proteins. *Proc. Natl. Acad. Sci. U. S. A. 74*, 2236−2240.
(49) Cooper, A., Johnson, C. M., Lakey, J. H., and Nöllmann, M. (2001) Heat does not come in different colours: entropy-enthalpy compensation, free energy windows, quantum confinement, pressure perturbation calorimetry, solvation and the multiple causes of heat capacity effects in biomolecular interactions. *Biophys. Chem. 93*, 215−230.
(50) Hilser, V. J., and Thompson, E. B. (2007) Intrinsic disorder as a mechanism to optimize allosteric coupling in proteins. *Proc. Natl. Acad. Sci. U. S. A. 104*, 8311−8315.
(51) Saavedra, H. G., Wrabl, J. O., Anderson, J. A., Li, J., and Hilser, V. J. (2018) Dynamic allostery can drive cold adaptation in enzymes. *Nature 558*, 324−328.
(52) Naganathan, A. N. (2019) Modulation of allosteric coupling by mutations: from protein dynamics and packing to altered native ensembles and function. *Curr. Opin. Struct. Biol. 54*, 1−9.

https://dx.doi.org/10.1021/acs.biochem.9b01006
Biochemistry 2020, 59, 790−801